Environmental Earth Sciences (2022) 81: 433
https://doi.org/10.1007/s12665-022-10555-x

ORIGINAL ARTICLE

Continuous three-dimensional stress monitoring in roof of coal mines for investigating the rockburst control effect with hydraulic fracturing

Hou Gao[1,2] · Wusheng Zhao[1] · Weizhong Chen[1] · Peiyao Xie[1,2] · Kun Zhong[1,2] · Changkun Qin[1,2]

Received: 20 January 2022 / Accepted: 13 August 2022 / Published online: 1 September 2022
© The Author(s), under exclusive licence to Springer-Verlag GmbH Germany, part of Springer Nature 2022

Abstract

The occurrence of rockburst in coal mines is closely related to the stress in coal and rock mass. Through hydraulic fracturing measurements in roof, the three-dimensional stress in roof before and after hydraulic fracturing as well as during working face advancing was monitored, and the effect of hydraulic fracturing in roof on controlling rockburst was studied. The test results show that (1) after hydraulic fracturing, the three principal stresses in roof decreased remarkably, whose maximum reduction was about 20%, while the elastic strain energy in roof decreased by about 31% as well; (2) as the working face advanced, the three principal stresses in roof in front of the working face would increase continuously until reaching peaks and induce the strata fracture, and the variation of the elastic strain energy in roof was basically consistent with that of the magnitude of the stress; (3) with hydraulic fracturing, the position of the peak stress moved from 11 to 21 m in front of the working face, the peaks of the three principal stresses decreased, whose maximum reduction was about 32%, and the peak of the elastic strain energy in roof also significantly decreased by about 51%. The field investigation shows that hydraulic fracturing in roof can release the stress and elastic strain energy in coal and rock mass instantaneously, and will reduce the risk of rockburst; hydraulic fracturing in roof can be an effective pre-destressing method to reduce the stress and energy concentration in coal and rock mass during mining, and will prevent the risk of rockburst.

Keywords Hydraulic fracturing · Rockburst · Roof · Three-dimensional stress · Elastic strain energy

Introduction

As the cornerstone of China's current energy, coal resources maintain the leading position of energy. With the continuous increase in mining depth and mining intensity of coal resources, the stress level of stopes keeps getting higher, so the rockburst disaster in coal mines is aggravating daily (Shi et al. 2020; Dai et al. 2021; Li et al. 2021), and has become one of the most important disasters affecting the safe production of coal mines, which seriously threatens the safety of underground personnel and equipment. For example, the "10.20" rockburst event of the Longyun coal mine in October 2018 and the "2.22" rockburst event of the Longgu coal mine in February 2020 caused 21 and 4 deaths, respectively, which greatly affected the normal production of mines and the safety of workers' lives and property.

At present, engineering measures to control rockburst mainly include assigning reasonable working face (Zhang et al. 2016; Zhu et al. 2016; Konicek et al. 2019), coal seam water injection (Holub et al. 2011; Guo et al. 2018; Pan et al. 2018), drilling pressure-released holes in coal seam (Li et al. 2014; Guo et al. 2017; Wang et al. 2019), blasting for pressure relief (Konicek et al. 2013; Kabiesz et al. 2015; Wojtecki et al. 2017; Yang et al. 2019), hydraulic fracturing (Fan et al. 2012; Yu 2016) and so on. Among them, hydraulic fracturing can smash the integrity of coal and rock mass, which has been widely used in the field of controlling rockburst in recent years.

Huang et al. (2011) conducted a theoretical analysis on the hydraulic fracturing of coal and rock mass, and believed that hydraulic fracturing could weaken the mechanical properties of coal and rock mass, so as to relieve the danger of rockburst. Through the analysis of microseismic monitoring data, Zhu et al. (2017) believed that hydraulic fracturing in

✉ Wusheng Zhao
wszhao@whrsm.ac.cn

1 State Key Laboratory of Geomechanics and Geotechnical Engineering, Institute of Rock and Soil Mechanics, Chinese Academy of Sciences, Wuhan 430071, China

2 University of Chinese Academy of Sciences, Beijing 100049, China

coal seam before mining could be used for rockburst prevention by reducing the stress and strain energy in rocks. Feng et al. (2015) believed that the mechanism of hydraulic fracturing in coal seam to prevent rockburst was increasing the resistance and releasing the energy of coal seam, and verified it by field observation, pipeline pressure, microseismic events and stress variation. Through field test research, Jiang et al. (2015) believed that hydraulic fracturing in coal seam could achieve rockburst prevention by means of "stress transfer, coal weakening and energy storage decrease". Liu et al. (2017) believed that hydraulic fracturing in coal seam could crack and dampen coal seam, so as to prevent rockburst. He et al. (2012) believed that hydraulic fracturing of roof could reduce abutment pressure and decrease tremor frequency as well as released energy thereby confirming the effect of roof hydraulic fracturing for rockburst prevention. Huang et al. (2018) believed that hydraulic fracturing of roof could weaken the impact effect by realizing pressure relief and stress transfer. Liu et al. (2020) believed that hydraulic fracturing of roof could promote fractures in roof, thereby avoiding the occurrence of rockburst. Jendryś et al. (2021) studied the hydraulic fracturing of roof by means of field microseismic observation and numerical simulation, and believed that hydraulic fracturing could reduce the frequency of high energy events and increase the frequency of low energy events, so as to prevent rockburst. However, due to the complexity of the field testing process of three-dimensional stress in coal and rock mass, and the high requirement of long-term stability of sensors for stress monitoring, there is little research on controlling rockburst of hydraulic fracturing based on three-dimensional stress in coal and rock mass. As for the stress monitoring in coal and rock mass, the coal seam stress monitoring technology (Kumar et al. 2019; Qiu et al. 2021; Rashed et al. 2021; Shen et al. 2020) is a common method, which is used to monitor the stress in coal seam. The stress obtained from the coal seam stress monitoring technology is usually one-dimensional stress. To monitor three-dimensional stress in rock mass, Stas et al. (2005) developed the compact conical ended borehole monitoring method device on the basis of the compact conical-ended borehole overcoring system (Obara and Sugawara 2003; Sugawara and Obara 1999). In addition, some useful results about three-dimensional stress monitoring in rock mass were gained using the compact conical ended borehole monitoring method probe (Konicek and Waclawik 2018; Lubosik et al. 2017; Ptáček et al. 2015; Stas et al. 2011) and other sensors (Yin et al. 2016; Zhao et al. 2020). However, these results do not involve hydraulic fracturing. Therefore, in this paper, through the field test of roof hydraulic fracturing, the three-dimensional stress in roof before and after hydraulic fracturing as well as during working face advancing was monitored by the FBG Stress Sensor. The results obtained from the field test complete the study of the variation of three-dimensional stress and elastic strain energy. This study quantifies the effect of roof hydraulic fracturing from the aspect of three-dimensional stress, and reveals its mechanism of controlling rockburst, which can provide a useful reference for the effectiveness evaluation of roof hydraulic fracturing and the control of rockburst.

Field investigation schemes

Overview of the test site

The 73L06 working face of the Jisan coal mine is selected as the hydraulic fracturing test site with Polish hydraulic fracturing equipment. The working face is located in the middle of the seventh mining area of the Jisan coal mine and is the first mining face of the third lower coal seam in the seventh mining area. The length of the 73L06 working face is 260 m, the advancing length is 1805 m, and the average buried depth is 825.48 m. The average thickness of the coal seam is 3.66 m with an average dip angle of 6°. The cross section of the two roadways in the 73L06 working face is rectangular, whose width and height are 4.8 m and 3.8 m, respectively. In addition, the direction of the roadways is 22° from north to east. The features of the roof and floor of the 73L06 working face are shown in Table 1. The basic roof is more thick and hard, with nearly horizontal bedding and oblique bedding. There are mainly 1 syncline and 9 normal faults within the 73L06 working face. The syncline amplitude is about 40 m, the throw of 2 normal faults is no more than 5.0 m, and the throw of the other 7 normal faults is no more than 1.4 m. Before mining of this working face, the rockburst hazard of the working face was analysed, and the

Table 1 Status table of the roof and floor

Position	Lithology	Average thickness (m)	Protodyakonov hardness
Basic roof	Medium sandstone and fine sandstone	9.94	6–10
Immediate roof	Siltstone, mudstone and fine siltstone	5.75	2–8
Immediate floor	Mudstone and siltstone	3.35	2–6
Basic floor	Fine sandstone and fine siltstone	8.56	4–8

results showed that the coal seam, roof and floor of the working face had weak rockburst tendency, and rockburst might occur during the mining process.

Monitoring scheme of three-dimensional stress in roof

According to the theory of rock mechanics (Amadei and Stephansson 1997), the stress in roof consists of two parts: in situ stress and induced stress. In situ stress, also called primitive stress, is the stress that exists in the roof prior to any disturbance (coal mining, roadway excavation, hydraulic fracturing, etc.). For a specific location, its value and direction remain the same. Induced stress, also called relative stress, is associated with artificial disturbances, such as coal mining, and its value and direction are constantly changing with the progress of artificial disturbance. Therefore, the three-dimensional real stress in roof σ_{ij} can be expressed as

$$\sigma_{ij} = \sigma_{ij}^{0} + \Delta\sigma_{ij} \tag{1}$$

where σ_{ij}^{0} is the in situ stress and $\Delta\sigma_{ij}$ is the induced stress.

The real stress state in roof has a direct effect on the deformation, instability and failure of roof, so it is especially important to monitor the three-dimensional real stress in roof. From Eq. (1), it can be seen that the three-dimensional real stress monitoring in roof can be completed in three steps: ① measuring the in situ stress in roof, ② monitoring the induced stress in roof, and ③ superposing the two to obtain the real stress in roof.

Because the resistance strain gauge sensors are susceptible to the interference of an underground strong electromagnetic field and have difficulty meeting the demands of long-term dynamic monitoring, the FBG Stress Sensor developed by the Institute of Rock and Soil Mechanics, Chinese Academy of Sciences, is adopted as the monitoring sensor. The FBG Stress Sensor mainly consists of a hollow cylinder, a piston and a positioning rod, as shown in Fig. 1. With an inner diameter of 34 mm and an outer diameter of 36 mm, the hollow cylinder is made of elastic steel possessing good elasticity and long-term stability. The hollow is used to place epoxy resin adhesive. The diameter of the piston is 33.5 mm, which is slightly less than the inner diameter of the hollow cylinder. There is an exit tube inside the piston, through which the adhesive placed in the hollow can be extruded. The front end of the positioning rod is a smooth cone, which is convenient for pushing the sensor in the borehole. With a length of 350 mm, the positioning rod can be cut to the right length according to the installation needs. There are 9 FBGs on the outer surface of the hollow cylinder, which can be used to measure the strain. In addition, a FBG is arranged

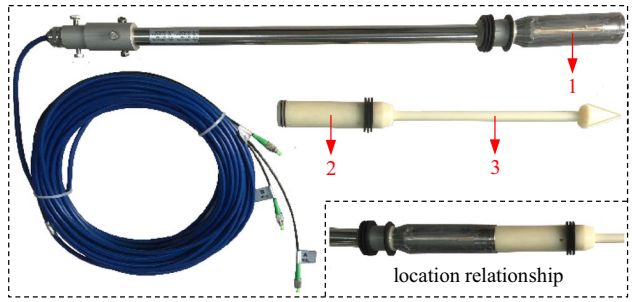

Fig. 1 FBG stress sensor, 1—hollow cylinder, 2—piston, and 3—positioning rod

inside the sensor to realize temperature compensation. The stress in rock can be obtained according to the strain measured by the sensor.

The overcoring stress measurement method is used to measure the in situ stress. First, a large hole is drilled at the monitoring position, and then a small hole is drilled at the bottom of the large hole. The borehole stress can be relieved after the FBG Stress Sensor is installed in the small hole. During the relief process, the strain of the borehole wall at the sensor location occurs due to the release of the in situ stress around the borehole. The in situ stress can be calculated by the variation of strain from the sensor.

The calculation method of the induced stress is the same as that of the in situ stress, except that there is no relief of the borehole stress after the sensor is installed in the small hole. As the roof stress changes due to artificial disturbances, such as hydraulic fracturing and coal mining, the strain of the borehole wall also changes. According to the strain change measured by the sensor, the induced stress can be calculated. The real stress can be obtained by adding the in situ stress and the induced stress.

Two monitoring sections are arranged in the 73L06 auxiliary haulage roadway. Monitoring sections I and II are located 1461 m and 1529 m away from the open-off cut, respectively, and a monitoring borehole is drilled at each monitoring section, as shown in Fig. 2. At the monitoring section I, the overcoring stress measurement method is first used to measure the in situ stress, and then the sensor is installed again to monitor the induced stress. As for the monitoring borehole at monitoring section I, its opening height is 3 m, its horizontal projection is vertical to the coal wall, and its angle of elevation is 30°. The borehole depth of the in situ stress measurement position is 13.4 m, beyond the influence range of the surrounding rock stress redistribution and meeting the requirement of in situ stress measurement. The borehole depth of the induced stress monitoring position is 13.8 m, located at the lower part of the basic roof. Since the two monitoring sections are very close, it can be considered that the in situ stress at the two monitoring sections is the

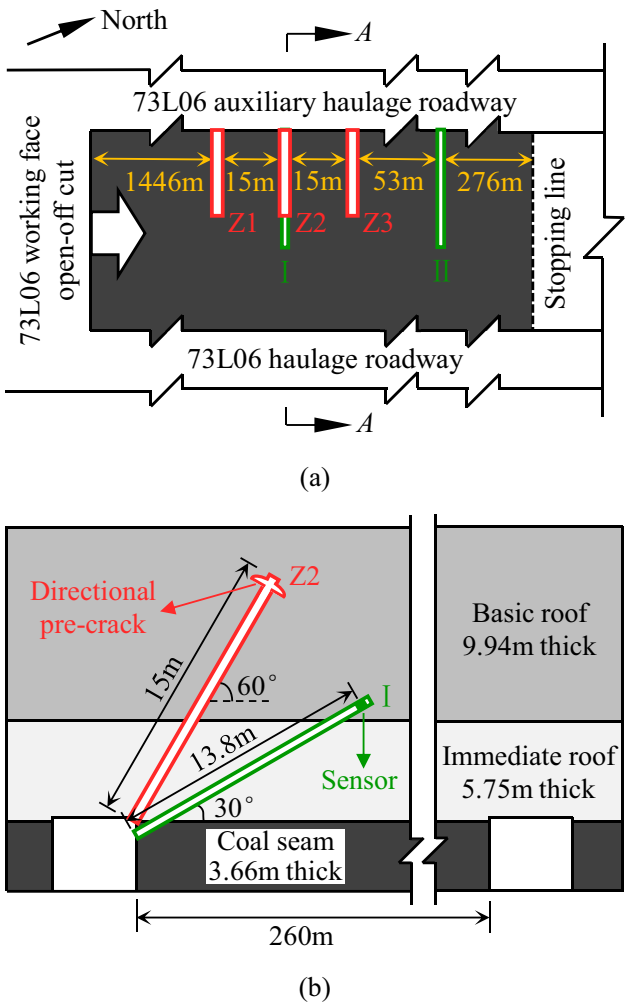

Fig. 2 Layout of the boreholes in the monitoring sections and the directional hydraulic fracturing boreholes. **a** Layout plan of the stress monitoring boreholes and the directional hydraulic fracturing boreholes, and **b** *A–A* section

same. Therefore, at monitoring section II, the borehole stress is not relieved, and only the induced stress is monitored. The monitoring position is 14.2 m deep, also located at the lower part of the basic roof. The other construction parameters of monitoring borehole II are the same as those of monitoring borehole I.

Roof hydraulic fracturing scheme

As a variant of hydraulic fracturing, directional hydraulic fracturing can reduce the difficulty of crack formation and control the direction of crack propagation by cutting directional pre-cracks in rock mass in advance. Directional hydraulic fracturing, therefore, is selected in the field test. In the light of the geological conditions of the 73L06 working face, the existing construction experience and the layout scheme of monitoring sections, the layout of directional hydraulic fracturing boreholes in roof is formulated. Three fracturing boreholes are arranged along the 73L06 auxiliary haulage roadway. As for the fracturing boreholes, their opening height is 3.8 m, their horizontal projection is vertical to the coal wall, their angle of elevation is 60°, their diameter is 48 mm, their depth is 15 m, and their sealing depth is 12 m. The fracturing section of boreholes, with a length of 3 m, is located at the middle of the basic roof. The three fracturing boreholes Z1, Z2 and Z3 are 1446 m, 1461 m and 1476 m away from the open-off cut, respectively, as shown in Fig. 2, among which the borehole Z2 is located directly above the monitoring borehole I. According to the geological conditions, the shortest horizontal distance between the fracturing boreholes and the main geological structures, namely, folds and faults, exceeds 200 m, and so do the monitoring boreholes. Thus, there is no obvious geological structure in the roof of interest. The steps of directional hydraulic fracturing can be summarized as follows: ① drilling fracturing boreholes, ② cutting the directional pre-crack at the bottom of boreholes, ③ fracturing the roof, and ④ recovering fracturing equipment. In the second of the above steps, the directional pre-crack is annular and perpendicular to the fracturing borehole, as shown in Fig. 2.

Test results and analysis

Field observation

The roof was hydraulically fractured after installing the sensors for monitoring stress. In the process of hydraulic fracturing, the boreholes Z1, Z2 and Z3 in Fig. 2 were fractured in sequence. During hydraulic fracturing, the sound of rock cracking could be heard near the boreholes. When fracturing the borehole Z1, no high-pressure water flowed out of the borehole, which indicated that the sealing effect was good. When fracturing the borehole Z2, there was no high-pressure water flowing out of the borehole. After about 9 min of water injection, the high-pressure water flowed out of the borehole Z1, similar to rainy conditions. When fracturing the borehole Z3, there was also no high-pressure water flowing out of the borehole. After about 7 min of water injection, the high-pressure water flowed out of the borehole Z2, similar to diversion. Given that the distance between adjacent boreholes is 15 m, it can be considered that the radius of hydraulic fracture propagation exceeds 7.5 m, and the effect of roof hydraulic fracturing is fairly good.

Fig. 3 Stress relief core

Table 2 In situ stress at the monitoring sections

Principal stresses	Magnitude (MPa)	Azimuth (°)	Dip angle (°)
σ_1	31.79	126.64	36.88
σ_2	20.85	14.22	26.95
σ_3	16.57	257.76	41.23

Positive principal stress indicates compression, positive azimuth indicates clockwise from the north, and positive dip angle indicates upwards from the horizontal

Three-dimensional stress in roof

In situ stress

The in situ stress at the monitoring sections was measured by the method of overcoring stress measurement. In addition, the stress relief core is shown in Fig. 3. According to the stress relief data, the in situ stress was calculated, as shown in Table 2.

Table 2 shows that the three principal stresses are at a certain angle to the horizontal, indicating that the roof at the monitoring sections is obviously affected by the tectonic stress field.

The working face coordinate system *O-xyz* is established on the basis of the 73L06 working face, where the positive *x*-direction points to the mining direction, parallel to the horizontal direction, the positive *z*-direction points up, and the *y*-direction is determined by the right-hand rule. In the working face coordinate system, the in situ stress is shown in Table 3.

Table 3 shows that the horizontal stress is relatively large, and the lateral pressure coefficients of the *x*-direction and *y*-direction are 0.90 and 1.12, respectively. The in situ stress is closely related to the roadway layout in mine design, and the maximum horizontal principal stress is often used to evaluate the stability of roadways. The larger the angle between the roadway and the maximum horizontal principal stress, the larger the roadway deformation, and the worse the roadway stability. The maximum horizontal principal stress is obtained in the working face coordinate system. In the horizontal plane, namely, the *xy* plane, the maximum horizontal principal stress is 27.00 MPa, and the angle between its orientation and the direction of the roadways in the 73L06 working face is 66.29°. The maximum horizontal principal stress is almost perpendicular to the roadways, which is not conducive to the stability of the roadways, so it is important to strengthen the roadway support.

Table 4 Three-dimensional stress in roof at section I after hydraulic fracturing

Principal stresses	Magnitude (MPa)	Azimuth (°)	Dip angle (°)
σ_1	25.45	135.62	46.96
σ_2	19.06	24.02	18.97
σ_3	14.68	279.07	36.88

Positive principal stress indicates compression, positive azimuth indicates clockwise from the north, and positive dip angle indicates upwards from the horizontal

Three-dimensional stress in roof after hydraulic fracturing

After the roof was hydraulically fractured, the three-dimensional stress in roof at monitoring section I changed significantly, as shown in Table 4, and the three-dimensional stress in roof at monitoring section II was basically unchanged, indicating that it was not affected by hydraulic fracturing. Given that the sensor at monitoring section I is 8.2 m away from the pre-crack of borehole Z2, and the sensor at monitoring section II is 53.6 m away from the pre-crack of borehole Z3, it can be proven that the influence radius of hydraulic fracturing is more than 8 m and less than 54 m.

The three principal stresses were still compressive stresses, as shown in Table 4. Comparing Tables 2 and 4, it can be seen that after hydraulic fracturing, the azimuths and dip angles of the three principal stresses changed slightly, but their values all decreased. The first, second and third principal stresses decreased by about 20%, 9%, and 11%, respectively. Roof hydraulic fracturing can effectively reduce the three-dimensional stress in roof, which has a good effect on pressure relief.

In the working face coordinate system, the three-dimensional stress in roof at monitoring section I is shown in

Table 3 In situ stress in the working face coordinate system

Stress components	σ_{xx}	σ_{yy}	σ_{zz}	τ_{xy}	τ_{yz}	τ_{zx}
Magnitude (MPa)	20.53	25.75	22.93	2.84	− 6.83	− 0.14

Positive normal stress indicates compression

Table 5 Three-dimensional stress in roof at section I in the working face coordinate system

Stress components	σ_{xx}	σ_{yy}	σ_{zz}	τ_{xy}	τ_{yz}	τ_{zx}
Magnitude (MPa)	19.40	18.90	20.90	1.70	− 4.97	− 0.81

Positive normal stress indicates compression

Table 5. Comparing Tables 3 and 5, it can be found that the normal stresses in the *x*-direction, *y*-direction and *z*-direction decreased by about 6%, 27% and 9%, respectively. Since the pre-crack is an annular crack perpendicular to the borehole, it can be inferred that the initial fracture surface is an annular surface perpendicular to the borehole axis. Considering the field observation and the arrangement of the three fracturing boreholes along the *x*-direction, it can be speculated that the direction of the final fracture surface is approximately parallel to the *x*-direction, and its dip angle is about 30°–40°. The stress is released due to the existence of the fracture surface. In addition, because the fracture surface is approximately parallel to the *x*-direction and at a certain angle to the horizontal, the influence of hydraulic fracturing on the *x*-direction is the least obvious, and the reduction range of normal stress in the *x*-direction is the smallest, while the influence on the *y*-direction is the most obvious, and the reduction range of normal stress in the *y*-direction is the largest. It can be found that roof hydraulic fracturing can significantly reduce the roof stress, and the reduction range of each stress component is affected by the orientation of the fracture surface.

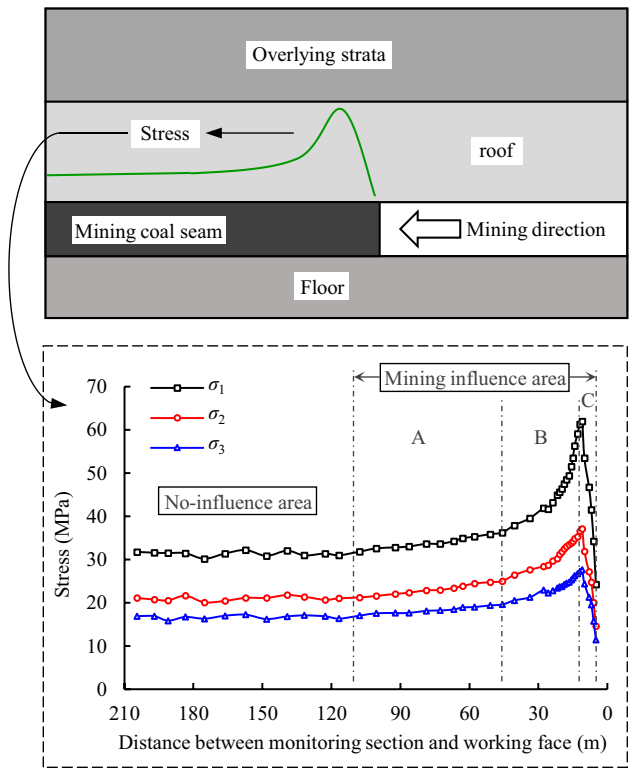

Fig. 4 Variation curves of the principal stresses in roof at section II

Three-dimensional stress variation in roof under the influence of mining

According to the relationship between time and advancement of the working face, the monitoring results varying with time are transformed to the relationship between stress and advancement of the working face, to facilitate engineering applications. Figure 4 shows the variation curves of the three-dimensional stress in roof at monitoring section II with the advancement of the working face. It can be seen from Fig. 4 that without being affected by hydraulic fracturing, the area in front of the working face can be divided into the mining no-influence area and the mining influence area, and the mining influence area can also be divided into three areas. The mining no-influence area is more than 110 m away from the working face, where the three-dimensional stress in roof is not affected by the disturbance of coal mining. The mining influence area is less than 110 m away from the working face. In the mining influence area, area *A* is the slow-growing area, located between 110 and 45 m away from the working face, where the mining influence begins to appear but is relatively weak, so the three principal stresses begin to increase slowly; area *B* is the rapid-growing area, located between 45 and 11 m away from the working face, where the mining influence is intensified, so the growth rate of three principal stresses is accelerated and the closer to the working face, the faster the growth rate is; area *C* is the sharp-declining area, located between 11 m and the monitoring end position (5 m) away from the working face, where the three principal stresses decrease sharply. The position of the peak stress is located 11 m in front of the working face, where the first principal stress is 61.94 MPa, increased by about 95%, the second principal stress is 37.13 MPa, increased by about 78%, and the third principal stress is 27.61 MPa, increased by about 67%.

Furthermore, the variation of the three-dimensional stress in roof at monitoring section II is analysed in the working face coordinate system, as shown in Fig. 5 (shear stress is omitted). It can be seen from Fig. 5 that under the influence of mining, the increase range of normal stress in the vertical direction is obviously greater than that in the two horizontal directions, indicating that the vertical stress plays a major role in rock deformation and strata behaviour.

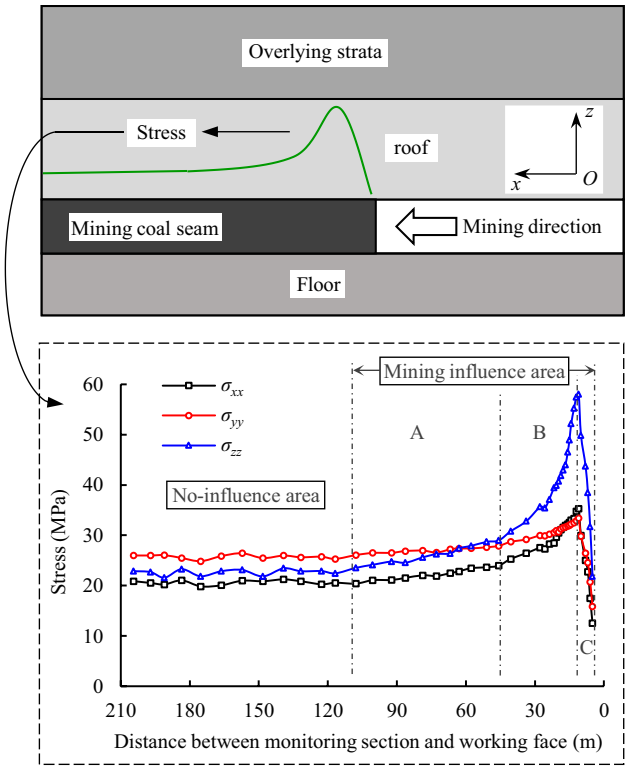

Fig. 5 Variation curves of the normal stresses in roof at section II in the working face coordinate system

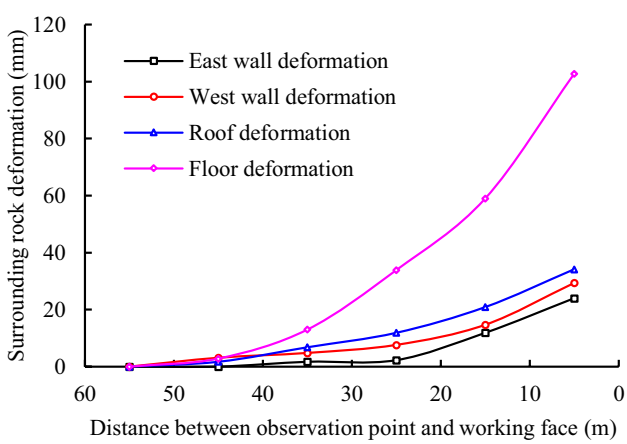

Fig. 6 Variation curves of the roadway surrounding rock deformation

Given that there is a corresponding relationship between stress and deformation, the deformation can characterize the stress state of the object. Therefore, to study the relationship between roof stress and coal seam stress, the surrounding rock deformation of the 73L06 auxiliary haulage roadway is analysed without the influence of hydraulic fracturing, as shown in Fig. 6. It can be seen from Fig. 6 that when the working face advances to 45 m away from the observation point, the deformation rate of the surrounding rock is accelerated, indicating that the mining influence is intensified so the growth rate of the coal seam stress is accelerated; the position of the maximum deformation rate of the surrounding rock is within 15 m in front of the working face, indicating that the peak stress in coal seam occurs within 15 m ahead of the working face. It can also be seen from Fig. 6 that the deformation of the roof or floor is greater than that of the sidewalls, which indicates that the vertical stress in surrounding rock plays a major role in the deformation of the roadway. The variation of surrounding rock deformation of the roadway is basically consistent with that of the three-dimensional stress in roof, which indicates that there is a good consistency between roof stress and coal seam stress.

Figure 7 shows the variation curves of the three-dimensional stress in roof at monitoring section I with the advancement of the working face. It can be found from Fig. 7 that after hydraulic fracturing, the mining influence area stays less than 110 m away from the working face, the boundary position between the slow-growing area and rapid-growing area increases to 50 m away from the working face, and the position of the peak stress moves to 21 m away from the working face. When the stresses reach the peaks, the first principal stress is 42.68 MPa, increased by about 68%, the second principal stress is 27.40 MPa, increased by about

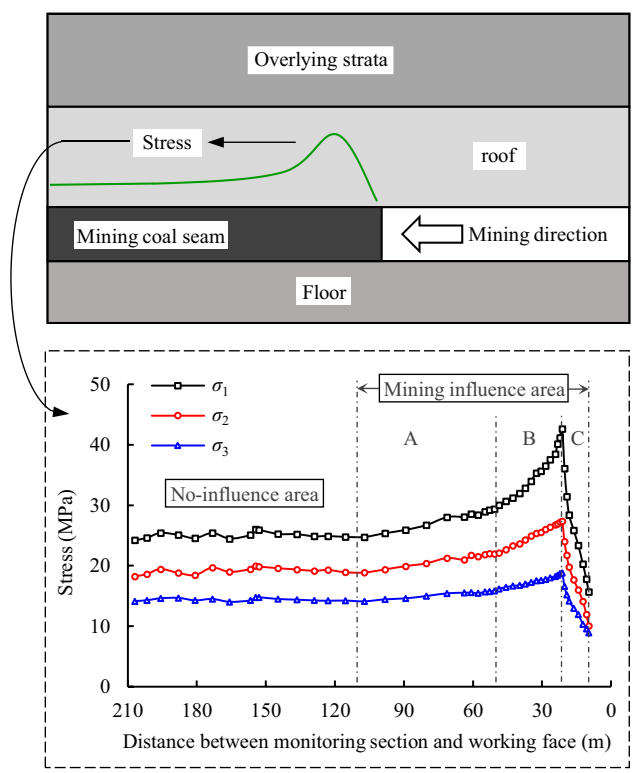

Fig. 7 Variation curves of the principal stresses in roof at section I

44%, and the third principal stress is 18.83 MPa, increased by about 28%.

It can be seen from Figs. 4 and 7 that the stress shows similar variation trends in the two figures. Due to coal mining, the pressure of overlying rock gradually transfers to the roof strata, so the three principal stresses in the roof strata increase continuously until reaching peaks, among which the first principal stress has the largest increase, the second principal stress has the second largest increase, and the third principal stress has the smallest increase. And then, the roof fractures, so the stress is released and the three principal stresses in the roof strata all begin to decrease sharply.

Comparing Figs. 4 and 7, it can be seen that with hydraulic fracturing, the position of the peak stress moves from 11 to 21 m in front of the working face, and the peaks of the three principal stresses all decrease in different degrees. The peak of the first principal stress decreases from 61.94 MPa to 42.68 MPa, reduced by about 31%; the peak of the second principal stress decreases from 37.13 MPa to 27.40 MPa, reduced by about 26%; the peak of the third principal stress decreases from 27.61 MPa to 18.83 MPa, reduced by about 32%. The results show that roof hydraulic fracturing can effectively reduce the three-dimensional stress peak in roof during coal mining.

Elastic strain energy in roof

The stress concentration in coal and rock mass causes energy accumulation, and the accumulation and release of energy in coal and rock mass is associated with the occurrence of rockburst. According to elastic mechanics, in principal stress space, the elastic strain energy stored by a unit volume of coal and rock mass, that is, the elastic strain energy density in coal and rock mass can be expressed as

$$U_e = \frac{1}{2E}\left[\sigma_1^2 + \sigma_2^2 + \sigma_3^2 - 2\mu\left(\sigma_1\sigma_2 + \sigma_2\sigma_3 + \sigma_3\sigma_1\right)\right] \quad (2)$$

where E is the elastic modulus of coal and rock mass; μ is Poisson's ratio of coal and rock mass; σ_1, σ_2 and σ_3 are the first, second and third principal stresses, respectively.

Elastic strain energy in roof before and after hydraulic fracturing

At the monitoring section I, before hydraulic fracturing, the elastic strain energy density in roof was 17.85 kJ/m^3; after hydraulic fracturing, the elastic strain energy density in roof was 12.35 kJ/m^3, reduced by about 31%. This shows that roof hydraulic fracturing can effectively release the elastic strain energy accumulated in the roof.

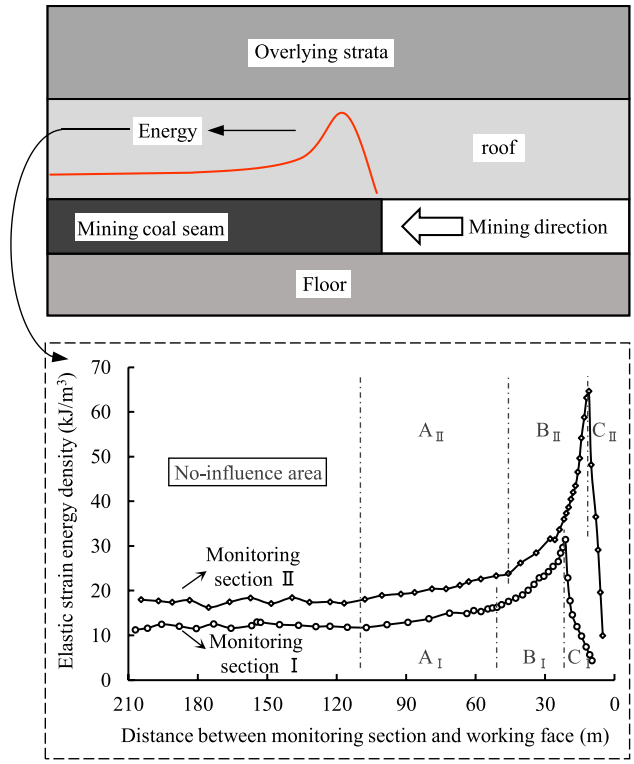

Fig. 8 Variation curves of the elastic strain energy density in roof

Elastic strain energy variation in roof under the influence of mining

Figure 8 shows the variation curves of the elastic strain energy density in roof at monitoring sections I and II with the advancement of the working face. It can be found from Fig. 8 that at the monitoring section II, the variation of the elastic strain energy is basically consistent with that of the magnitude of the stress. The area in front of the working face can be divided into the mining no-influence area and the mining influence area, and the mining influence area can be divided into the slow-growing area (between 110 and 45 m away from the working face), the rapid-growing area (between 45 and 11 m away from the working face) and the sharp-declining area (between 11 m and the monitoring end position away from the working face). The peak of the elastic strain energy density is 64.64 kJ/m^3, increased by about 262%. At the monitoring section I, the variation of the elastic strain energy is also basically consistent with that of the magnitude of the stress, and the peak of the elastic strain energy density is 31.45 kJ/m^3, increased by about 155%.

Comparing the two curves in Fig. 8, it can be found that with hydraulic fracturing, the peak of the elastic strain

energy density in roof decreases from 64.64 to 31.45 kJ/m^3, reduced by about 51%, which indicates that roof hydraulic fracturing can effectively reduce the maximum elastic energy storage in roof during coal mining.

Mechanism of controlling rockburst of roof hydraulic fracturing

The occurrence mechanism of rockburst is the theoretical basis of research on controlling rockburst. At present, the widely used occurrence mechanisms mainly include strength theory, energy theory, stiffness theory and so on.

Mechanism of controlling rockburst based on strength theory

The essence of rockburst in coal mines is the sudden instability and failure of coal and rock mass under a high stress state. The problem of rockburst is actually the problem of stress in coal and rock mass (Qi et al. 2013). According to strength theory, when the stress in coal and rock mass exceeds its ultimate strength, rockburst disasters will occur.

The test results show that roof hydraulic fracturing can effectively reduce the three-dimensional stress in roof and the stress peak in roof during mining. Given that the coal seam stress has a good consistency with the roof stress, it can be inferred that roof hydraulic fracturing can also effectively reduce the coal seam stress and the coal seam stress peak in the mining process. Therefore, on the one hand, roof hydraulic fracturing can achieve pressure relief of coal and rock mass, thereby relieving the danger of rockburst on the spot. On the other hand, roof hydraulic fracturing can also avoid the high stress state of coal and rock mass, thereby preventing rockburst.

Mechanism of controlling rockburst based on energy theory

When a unit volume of coal and rock mass deforms under the external force, assuming that there is no heat exchange with the external environment in the whole process, according to the law of conservation of energy, the total energy U inputted by external force work can be expressed as (Chen et al. 2009; Meng et al. 2018)

$$U = U_e + U_d \tag{3}$$

where U_e is the elastic strain energy in coal and rock mass that can be released under certain conditions; U_d is the dissipated strain energy in coal and rock mass.

According to energy theory, when the elastic strain energy U_e reaches the energy U_0 required for the instability and failure of coal and rock mass, the instability and failure of coal and rock mass will occur. When $U_e = U_0$, the static instability and failure of coal and rock mass will occur; when $U_e > U_0$, the dynamic instability and failure of coal and rock mass will occur, and the energy difference $\Delta = U_e - U_0$ will be released in the form of kinetic energy.

The test results show that roof hydraulic fracturing can effectively reduce the elastic strain energy in roof and the maximum elastic energy storage in roof during mining. Given that the elastic strain energy is obtained from the stress calculation and the coal seam stress has a good consistency with the roof stress, it can also be inferred that roof hydraulic fracturing can effectively reduce the elastic strain energy in coal seam and the maximum elastic energy storage in coal seam during mining. Therefore, on the one hand, roof hydraulic fracturing can reduce the accumulation of elastic strain energy in coal and rock mass, thereby relieving the danger of rockburst on the spot. On the other hand, roof hydraulic fracturing can also avoid the high energy state of coal and rock mass, thereby preventing rockburst.

In summary, the mechanism of controlling rockburst of roof hydraulic fracturing is as follows:

(1) Mechanism of preventing rockburst: reducing the three-dimensional stress peak and the maximum elastic energy storage in coal and rock mass during mining.
(2) Mechanism of relieving the danger of rockburst: releasing the three-dimensional stress and the elastic strain energy in coal and rock mass instantaneously.

Conclusions

In this paper, a field test of roof hydraulic fracturing in a coal mine was conducted. Through the field test, the three-dimensional stress in roof before and after hydraulic fracturing as well as during working face advancing was monitored, and not only the variation of the three-dimensional stress and elastic strain energy but also the mechanism of controlling rockburst of roof hydraulic fracturing was studied. The conclusions are as follows:

(1) After hydraulic fracturing, the azimuths and dip angles of the three principal stresses in roof change slightly, but the values all decrease remarkably and the maximum reduction is about 20%; the elastic strain energy in roof also obviously decreases by about 31%.
(2) With the advancement of the working face, the three principal stresses in roof in front of the working face

increase continuously until reaching peaks. Thereafter, the roof begins to fracture, and the three principal stresses decrease sharply. The variation of the elastic strain energy in roof is basically consistent with that of the magnitude of the stress.

(3) With hydraulic fracturing, the mining influence area, which is less than 110 m away from the working face, is basically unchanged, the position of the peak stress moves from 11 to 21 m in front of the working face, and the peaks of the three principal stresses all decrease in varying degrees, whose maximum reduction is about 32%; the peak of the elastic strain energy in roof also significantly decreases by about 51%.

(4) The mechanism of controlling rockburst of roof hydraulic fracturing can be divided into mechanism of preventing rockburst and mechanism of relieving the danger of rockburst, among which the former is reducing the three-dimensional stress peak and the maximum elastic energy storage in coal and rock mass during mining, and the latter is releasing the three-dimensional stress and the elastic strain energy in coal and rock mass instantaneously.

Acknowledgements This work was supported by the National Natural Science Foundation of China (Grant numbers 51991393 and 52079134).

Funding National Natural Science Foundation of China, 51991393, Wusheng Zhao, 52079134, Wusheng Zhao.

Declarations

Conflict of interest The authors declare that they have no conflict of interest.

References

Amadei B, Stephansson O (1997) Rock stress and its measurement. Chapman & Hall, London

Chen WZ, Lu SP, Guo XH, Qiao CJ (2009) Research on unloading confining pressure tests and rockburst criterion based on energy theory. Chin J Rock Mech Eng 28(8):1530–1540 (**in Chinese**)

Dai LP, Pan YS, Li ZH, Wang AW, Xiao YH, Liu FY, Shi TW, Zheng WH (2021) Quantitative mechanism of roadway rockbursts in deep extra-thick coal seams: theory and case histories. Tunn Undergr Space Technol 111:103861. https://doi.org/10.1016/j.tust.2021.103861

Fan J, Dou LM, He H, Du TT, Zhang SB, Gui B, Sun XL (2012) Directional hydraulic fracturing to control hard-roof rockburst in coal mines. Int J Min Sci Technol 22(2):177–181. https://doi.org/10.1016/j.ijmst.2011.08.007

Feng Y, Jiang FX, Zhai MH, Wang B, Guo XS, Cheng G (2015) Mechanism of the fixed-point hydraulic fracturing method for preventing rockburst in coalseam. Rock Soil Mech 36(4):1174–1181, in Chinese. https://doi.org/10.16285/j.rsm.2015.04.035

Guo WY, Zhao TB, Tan YL, Yu FH, Hu SC, Yang FQ (2017) Progressive mitigation method of rock bursts under complicated geological conditions. Int J Rock Mech Min Sci 96:11–22. https://doi.org/10.1016/j.ijrmms.2017.04.011

Guo WY, Tan YL, Yang ZL, Zhao TB, Hu SC (2018) Effect of saturation time on the coal burst liability indexes and its application for rock burst mitigation. Geotech Geol Eng 36:589–597. https://doi.org/10.1007/s10706-017-0300-2

He H, Dou LM, Fan J, Du TT, Sun XL (2012) Deep-hole directional fracturing of thick hard roof for rockburst prevention. Tunn Undergr Space Technol 32:34–43. https://doi.org/10.1016/j.tust.2012.05.002

Holub K, Rušajová J, Holečko J (2011) Particle velocity generated by rockburst during exploitation of the longwall and its impact on the workings. Int J Rock Mech Min Sci 48(6):942–949. https://doi.org/10.1016/j.ijrmms.2011.05.004

Huang BX, Cheng QY, Liu CY, Wei MT, Fu JH (2011) Hydraulic fracturing theory of coal-rock mass and its technical framework. J Min Safety Eng 28(2):167–173 (**in Chinese**)

Huang BX, Liu JW, Zhang Q (2018) The reasonable breaking location of overhanging hard roof for directional hydraulic fracturing to control strong strata behaviors of gob-side entry. Int J Rock Mech Min Sci 103:1–11. https://doi.org/10.1016/j.ijrmms.2018.01.013

Jendryś M, Hadam A, Ćwiękała M (2021) Directional hydraulic fracturing (DHF) of the roof, as an element of rock burst prevention in the light of underground observations and numerical modelling. Energies 14(3):562. https://doi.org/10.3390/en14030562

Jiang FX, Wang B, Zhai MH, Guo XS, Huang GW, Huang JR (2015) Field tests on fixed-point hydraulic fracture with extra-high pressure in coal seam for rock burst prevention. Chin J Geotech Eng 37(3):526–531 in Chinese. https://doi.org/10.11779/CJGE201503017

Kabiesz J, Lurka A, Drzewiecki J (2015) Selected methods of rock structure disintegration to control mining hazards. Arch Min Sci 60(3):807–824. https://doi.org/10.1515/amsc-2015-0053

Konicek P, Waclawik P (2018) Stress changes and seismicity monitoring of hard coal longwall mining in high rockburst risk areas. Tunn Undergr Space Technol 81:237–251. https://doi.org/10.1016/j.tust.2018.07.019

Konicek P, Soucek K, Stas L, Singh R (2013) Long-hole destress blasting for rockburst control during deep underground coal mining. Int J Rock Mech Min Sci 61:141–153. https://doi.org/10.1016/j.ijrmms.2013.02.001

Konicek P, Ptacek J, Waclawik P, Kajzar V (2019) Long-term Czech experiences with rockbursts with applicability to today's underground coal mines. Rock Mech Rock Eng 52:1447–1458. https://doi.org/10.1007/s00603-018-1489-y

Kumar A, Waclawik P, Singh R, Ram S, Korbel J (2019) Performance of a coal pillar at deeper cover: field and simulation studies. Int J Rock Mech Min Sci 113:322–332. https://doi.org/10.1016/j.ijrmms.2018.10.006

Li ZL, Dou LM, Cai W, Wang GF, He J, Gong SY, Ding YL (2014) Investigation and analysis of the rock burst mechanism induced within fault-pillars. Int J Rock Mech Min Sci 70:192–200. https://doi.org/10.1016/j.ijrmms.2014.03.014

Li XL, Chen SJ, Wang EY, Li ZH (2021) Rockburst mechanism in coal rock with structural surface and the microseismic (MS) and electromagnetic radiation (EMR) response. Eng Fail Anal 124:105396. https://doi.org/10.1016/j.engfailanal.2021.105396

Liu JW, Liu CY, Yao QL, Si GY (2020) The position of hydraulic fracturing to initiate vertical fractures in hard hanging roof for stress relief. Int J Rock Mech Min Sci 132:104328. https://doi.org/10.1016/j.ijrmms.2020.104328

Liu JH, Yang WL, Jiang FX, Guo XS (2017) Mechanism of cracking-before-injecting method to prevent coal burst and its field test. Chin J Rock Mech Eng 36(12):3040–3049 in Chinese. https://doi.org/10.13722/j.cnki.jrme.2017.0206

Lubosik Z, Waclawik P, Horak P, Wrana A (2017) The influence of in-situ rock mass stress conditions on deformation and load of gateroad supports in hard coal mine. Proc Eng 191:975–983. https://doi.org/10.1016/j.proeng.2017.05.269

Meng QB, Zhang MW, Zhang ZZ, Han LJ, Pu H (2018) Experimental research on rock energy evolution under uniaxial cyclic loading and unloading compression. Geotech Test J 41(4):717–729. https://doi.org/10.1520/GTJ20170233

Obara Y, Sugawara K (2003) Updating the use of the CCBO cell in Japan: overcoring case studies. Int J Rock Mech Min Sci 40(7–8):1189–1203. https://doi.org/10.1016/j.ijrmms.2003.07.007

Pan JF, Liu SH, Wang SW, Xia YX (2018) A new theoretical view of rockburst and its engineering application. Adv Civ Eng. https://doi.org/10.1155/2018/4683457

Ptáček J, Konicek P, Staš L, Waclawik P, Kukutsch R (2015) Rotation of principal axes and changes of stress due to mine-induced stresses. Can Geotech J 52:1440–1447. https://doi.org/10.1139/cgj-2014-0364

Qi QX, Li XL, Zhao SK (2013) Theory and practices on stress control of mine pressure bumping. Coal Sci Tech 41(6):1–5 in Chinese. https://doi.org/10.13199/j.cst.2013.06.7.qiqx.007

Qiu PQ, Ning JG, Wang J, Hu SC, Li Z (2021) Mitigating rock burst hazard in deep coal mines insight from dredging concentrated stress: a case study. Tunn Undergr Space Technol 115:104060. https://doi.org/10.1016/j.tust.2021.104060

Rashed G, Mohamed K, Kimutis R (2021) A coal rib monitoring study in a room-and-pillar retreat mine. Int J Min Sci Technol 31(1):127–135. https://doi.org/10.1016/j.ijmst.2020.10.001

Shen BT, Duan Y, Luo X, van de Werken M, Dlamini B, Chen L, Vardar O, Canbulat I (2020) Monitoring and modelling stress state near major geological structures in an underground coal mine for coal burst assessment. Int J Rock Mech Min Sci 129:104294. https://doi.org/10.1016/j.ijrmms.2020.104294

Shi XF, Zhang XK, Jiang FX, Wang H, Wei J (2020) Study on practice of rockburst accident prevention in multi-seam mining controlled by large fault and hard roof. Geotech Geol Eng 38:6843–6853. https://doi.org/10.1007/s10706-020-01473-5

Stas L, Knejzlik J, Palla L, Soucek K, Waclawik P (2011) Measurement of stress changes using a compact conical-ended borehole monitoring. Geotech Test J 34(6):685–693. https://doi.org/10.1520/GTJ102794

Stas L, Knejzlik J, Rambousky Z (2005) Conical strain gauge probes for stress measurement. In: Proceedings of the Int Symposium of the ISRM, EUROCK, Impact of human activity on the geological environment, Brno, Czech Rep, pp 587–592

Sugawara K, Obara Y (1999) Draft ISRM suggested method for in situ stress measurement using the compact conical-ended borehole overcoring (CCBO) technique. Int J Rock Mech Min Sci 36:307–322

Wang GF, Gong SY, Dou LM, Cai W, Yuan XY, Fan CJ (2019) Rockburst mechanism and control in coal seam with both syncline and hard strata. Saf Sci 115:320–328. https://doi.org/10.1016/j.ssci.2019.02.020

Wojtecki Ł, Mendecki MJ, Zuberek WM (2017) Determination of destress blasting effectiveness using seismic source parameters. Rock Mech Rock Eng 50:3233–3244. https://doi.org/10.1007/s00603-017-1297-9

Yang J, He MC, Cao C (2019) Design principles and key technologies of gob side entry retaining by roof pre-fracturing. Tunn Undergr Space Technol 90:309–318. https://doi.org/10.1016/j.tust.2019.05.013

Yin HY, Lefticariu L, Wei JC, Guo JB, Li ZJ, Guan YZ (2016) In situ dynamic monitoring of stress revolution with time and space under coal seam floor during longwall mining. Environ Earth Sci 75:1249. https://doi.org/10.1007/s12665-016-6071-x

Yu B (2016) Behaviors of overlying strata in extra-thick coal seams using top-coal caving method. J Rock Mech Geotech Eng 8(2):238–247. https://doi.org/10.1016/j.jrmge.2015.11.006

Zhang JF, Jiang FX, Zhu ST, Zhang L (2016) Width design for gobs and isolated coal pillars based on overall burst-instability prevention in coal mines. J Rock Mech Geotech Eng 8(4):551–558. https://doi.org/10.1016/j.jrmge.2015.12.006

Zhao WS, Zhong K, Chen WZ (2020) A fiber Bragg grating borehole deformation sensor for stress measurement in coal mine rock. Sensors 20(11):3267. https://doi.org/10.3390/s20113267

Zhu ST, Feng Y, Jiang FX (2016) Determination of abutment pressure in coal mines with extremely thick alluvium stratum: a typical kind of rockburst mines in China. Rock Mech Rock Eng 49:1943–1952. https://doi.org/10.1007/s00603-015-0868-x

Zhu QJ, Feng Y, Cai M, Liu JH, Wang HH (2017) Interpretation of the extent of hydraulic fracturing for rockburst prevention using microseismic monitoring data. J Nat Gas Sci Eng 38:107–119. https://doi.org/10.1016/j.jngse.2016.12.034

Publisher's Note Springer Nature remains neutral with regard to jurisdictional claims in published maps and institutional affiliations.

Springer Nature or its licensor holds exclusive rights to this article under a publishing agreement with the author(s) or other rightsholder(s); author self-archiving of the accepted manuscript version of this article is solely governed by the terms of such publishing agreement and applicable law.